Structure and Dynamics of the ApA, ApC, CpA, and CpC RNA Dinucleoside Monophosphates Resolved with NMR Scalar Spin−Spin Couplings

Zuzana Vokáčová,*,† Miloš Buděšínský,*,† Ivan Rosenberg,*,† Bohdan Schneider,§ Jiří Šponer,‡ and Vladimír Sychrovský*,†,‡

Institute of Organic Chemistry and Biochemistry, v.v.i., Academy of Sciences of the Czech Republic, Flemingovo náměstí 2, 166 10 Prague 6, Czech Republic, Institute of Biophysics, v.v.i., Academy of Sciences of the Czech Republic, Královopolská 135, 612 65 Brno, Czech Republic, and Institute of Biotechnology AS CR, v.v.i., Vídeňská 1083, 146 20 Prague, Czech Republic

Received: November 5, 2008

The measured NMR scalar coupling constants (*J*-couplings) in the XpY, (X,Y = adenine (A) or cytosine (C)) RNA dinucleoside monophosphates (DMPs) were assigned to the backbone (α, β, γ, δ, ε, ζ) and glycosidic (χ) torsion angles in order to resolve the global structure of the DMP molecules. The experimental *J*-couplings were correlated with the theoretical *J*-couplings obtained as the dynamical averages of the Karplus equations relevant to the torsion angles. The dynamical information was captured using the molecular dynamics (MD) calculation method. The individual conformational flexibility of the four DMP molecules was thus consistently probed with the NMR *J*-couplings. The calculated structure and flexibility of the DMP molecules depend on the sequence considered with respect to the 5′ and 3′ end of the DMP molecules (5′-XpY-3′). The dynamical characteristics of the two nucleosides are not equivalent even for the ApA and CpC homologues. An enhancement of the sampling in the MD calculations was achieved using five different starting structural motives classified previously for the RNA backbone in the solid phase (Richardson et al. *RNA* 2008, *14*, 465−481). The initial structures were selected on the basis of a database search for RNA oligonucleotides. Frequent interconversions between the conformers during the MD calculations were actually observed. The structural interpretation of the NMR spectroscopic data based on the MD simulations combined with the Karplus equations indicates that the dominant conformation of the DMP molecules in solution corresponds to the A-RNA form. For ∼52% of the total simulation time (∼1000 ns), the ζ(g−)−α(g−)-γ(g+) backbone topology corresponding to the canonical A-RNA form was observed, with roughly equally populated C2′- and C3′-*endo* sugar puckers interconverting on the nanosecond time scale. However, other noncanonical patterns were also found and thus indicate their relatively high potential to be populated in the dynamical regime. For ∼72% of the time portion when the A-RNA of the $\zeta-\alpha-\gamma$ combination occurred, the nucleobases were classified as being mutually stacked. The geometries of the nucleobases classified in this work as stacked were significantly more populated for the DMP molecules with adenosine at the 3′ end (ApA and CpA DMPs) than the ApC or CpC RNA molecules with C at the 3′ end.

Introduction

Nucleic acids (DNA and RNA) are among the most important classes of biomolecules. DNA is responsible for the storage and coding of genetic information. For quite a long time, the role of RNA was underestimated. However, the astonishing discovery of RNA enzymes (ribozymes) less than 30 years ago[1] signaled a much wider than expected range of RNA's functional capabilities. After the revelation of the RNA catalytic function, major discoveries of new RNA roles and functional capabilities came one after another. These findings revolutionalized the biosciences, ultimately identifying the central role of RNA in biology and evolution. We now know that RNA is intimately involved in literally every aspect of cellular life. RNA molecules are integral components of the cellular machinery for protein synthesis and transport, RNA editing and splicing, and chromosome replication and regulation and possess many other functions. RNA thus functions as an information carrier, catalyst, and regulatory element, most likely reflecting its importance in the earliest stages of evolution (The RNA World).[2]

Among the recent major advances, we should mention the discovery of the RNA interference[3] and the solution of near-atomic resolution X-ray structures of several ribosomal subunits and ribosomes.[4−11] These structures have provided astonishing insights into the complexity of the architectures of large functional RNAs, the principles of RNA base pairing (strikingly different from DNA), the modularity of functional RNAs, and so forth. X-ray crystallography has been complemented by cryoelectromicroscopy (CryoEM) studies. CryoEM does not achieve atomic resolution but is very versatile and can capture many more conformational substates of this fascinating molecular machine.[12−14] Notably, the two structural experimental methods above provide basically static averaged pictures of the RNAs and RNA-based molecular machines. However, in order to understand RNA functions and folding fully, dynamical information is needed.[15] It is of primary importance to understand the dynamics and fluctuations of RNAs as molecular machines like ribosomes are stochastic machines working in

* To whom correspondence should be addressed.
† Institute of Organic Chemistry and Biochemistry, Academy of Sciences of the Czech Republic.
‡ Institute of Biophysics, Academy of Sciences of the Czech Republic.
§ Institute of Biotechnology AS CR.

10.1021/jp809762b CCC: $40.75
Published on Web 01/07/2009

the regime of high viscosity and thermal fluctuations. Biomolecular machines convert the energy of thermal fluctuations into functional movements.[16] Many of the functional capabilities of RNA are based on its chemical properties.

At first glance, these properties may appear rather limited due to the monotony of RNA chemical building blocks, comprising only four nucleotides; nevertheless, RNA typically folds into complex three-dimensional (tertiary) structures. The subtle placement of the functional groups and their structural dynamics determine the RNA's functions. RNA's conformational variability is astonishing and larger than that observed in DNA molecules. RNAs are organized via hierarchical principles. The 2D structure and thermodynamic stability are basically determined by canonical Watson−Crick base pairing of the A-RNA segments.[17,18] Further, RNA molecules utilize a wide range of noncanonical recurrent structural motifs, building blocks, and tertiary interaction patterns, often characterized by salient sequence, 2D and 3D signatures, which means that they fold into highly specific three-dimensional architectures strongly related to their biological functions.[19−24]

Vital information on the RNA structure and dynamics can be obtained with NMR spectroscopy,[25−31] which has become one of the leading techniques in that field. Theoretical MD simulations often complement the experimental insights by a detailed analysis of the stochastic fluctuations and flexibility of RNA molecules on the ∼1−1000 ns time scale.[32−36]

The structural parameters of the nucleic acids resolved with the NMR spectroscopy technique may utilize different NMR parameters.[37−39] The proton−proton distances can typically be obtained by measuring the nuclear Overhauser enhancement (NOE). The applicability of NOE in nucleic acids is, however, rather limited due to the scarcity of the relevant protons.[37] The ^{1}H, ^{13}C, and ^{31}P shifts can provide structural information that is unfortunately confined to a close proximity of the probed nucleus. Accurate interpretation of the NMR shifts in terms of long-distance structural restraints may thus become difficult. For example, the ^{31}P shifts of the phosphate group vary by only a few ppm despite the large structural variation in the nucleic acid backbone.[40] One of the long-distance structural restraints in nucleic acids can be obtained with the scalar *J*-couplings measured along a chain of covalently bound atoms[41] or across the noncovalent contacts.[42,43] The three-bond *J*-couplings (the ^{3}J-couplings) correlated with the magnitude of the corresponding torsion angels[44,45] are thus well suited for structural (conformational) studies of nucleic acids.[41] The specificity of the set of *J*-couplings assigned to individual torsion angles along the RNA backbone with respect to its conformational patterns had been shown also theoretically.[46] Another long-distance structural restraint can be obtained with the cross-correlated relaxation rates recently utilized in NMR studies of nucleic acids.[47,48]

This work was motivated by the scarcity of detailed structural information available for short RNA oligonucleotides, which were recognized as increasingly important in the RNA regulatory processes of gene expression briefly mentioned above. The structural characteristics of RNA molecules such as the dependence of flexibility on the sequence (the role of the base-stacking phenomena in the stabilization of short single-strand RNA molecules), and other conditions like various solvent compositions, are essential for understanding the biological function of the molecules. The present joint experimental and theoretical study was therefore particularly focused on (a) the determination of the local structure in terms of torsion angles resolved solely on the basis of measured *J*-couplings (with a consistent set of NMR parameters), (b) a complementary MD study providing the dynamical interpretation of the measured *J*-couplings in terms of the distribution functions modeled for the torsion angles, (c) the assembly of the local structural information captured for the individual torsions aiming at the global resolution of the RNA conformational patterns (this point can also be classified as a backward validation of the MD calculations method including the force field used), and (d) a detailed analysis of the global RNA topologies resolved with the NMR data for the ApA, ApC, CpA, and CpC RNA dinucleoside monophosphates, addressing particularly the relation between the various topologies of the RNA backbone and base stacking via the sequential permutations of the A (purine) and C (pyrimidine) nucleobases (the A and C nucleobases in the synthesized model compounds were selected on purpose because of their different proposed abilities for base stacking[49]).

Methods Section

The 3′,5′-Linked DMP Molecules. These molecules were synthesized in the solid phase on a 30 μmol scale by a standard phosphoramidite procedure using commercially available amidites and CPG solid supports. After deprotection, the dimers were purified by RP HPLC on a Luna C18 (2) column (5 μm, 10 × 250 mm; Phenomenex, U.S.A.) in an aqueous 0.1 M triethylammoniumbicarbonate buffer. The obtained compounds were transformed into sodium salts on Dowex 50 (Na^{+}) and finally adjusted by lyophilization from water.

NMR Spectra. The NMR spectra of dinucleoside monophosphates ApA, ApC, CpA, and CpC were measured on a Bruker AVANCE-II instrument (^{1}H at 600.13 MHz and ^{13}C at 150.9 MHz) using a 5 mm TXI cryoprobe in D_2O at a temperature of 280 K (320 K for the CpC DMP molecule). Chemical shifts were obtained from the 1D-^{1}H and ^{13}C NMR spectra, referenced to internal dioxane (1 drop added to D_2O solution) and recalculated to the δ-scale using $\delta_H = 3.75$ and $\delta_C = 69.3$ for dioxane. The homonuclear 2D-H,H-COSY and 2D-H,H-ROESY spectra were used for the structural assignment of hydrogen signals and heteronuclear correlated 2D-H,C-HSQC and 2D-H,C-HMBC spectra for the assignment of the carbon signals. The *J*-coupling constants *J*(H,H) and *J*(H,P) were obtained from 1D resolution-enhanced ^{1}H spectra, *J*(C,P) from proton-decoupled ^{13}C NMR spectra, and vicinal *J*(C,H) between H-1′ and the corresponding carbon atom of adenine or cytosine from nondecoupled ^{13}C NMR spectra.

Molecular Dynamics. MD simulations were carried out with the AMBER program, version 8,[50] using the AMBER parm99[51] force field. The RNA molecules were embedded in explicit water (a box of 31 Å × 31 Å × 30 Å with roughly 800 TIP3P water molecules). Prior to the MD simulations (50 ns, periodic boundary conditions, a temperature of 300 K, a cutoff at 10 Å), a four-step equilibration was carried out: (1) a solvent relaxation with a rigid geometry of the RNA molecules (500 steps of the steepest descent algorithm followed by 1000 steps of the conjugate gradient minimization), (2) a steepest descent (1000 steps) followed by a conjugate gradient minimization of the RNA backbone (1500 steps), (3) a heating/equilibration simulation at constant volume and a restrained RNA backbone with a temperature increase from 0 to 300 K (20 ps, with the force constant for the backbone torsions being 80 kcal·mol^{-1}·Å^{-2}, a 2 fs time step, SHAKE algorithm, with the constrained bonds involving hydrogen), and (4) a final equilibration (100 ps, constant pressure, no restraints, SHAKE algorithm). The total simulation time for one DMP molecule was 250 ns (five initial structural patterns with production runs of 50 ns for each starting geometry). For the CpC RNA

molecule, the calculation was performed at a higher temperature of 340 K using the same protocol.

Distribution Functions. The distribution functions for the torsion angles were calculated from their evolution during the MD calculations. The interval of 0−360° for each torsion angle was divided into 36 subintervals of equal size. The number of geometries (snap shots) with the values of the given torsion angle in each subinterval was accumulated along the trajectory (N_i, $i = 1,..., 36$). The normalized distributions ($n_i = N_i/(\sum N_i)$) were used for the numerical integration of the Karplus-like equations. It should be mentioned that the calculated values of the averaged *J*-couplings changed by less than 0.01 Hz when the finer grid (72 subintervals of equal size) was used in the same numerical integration procedure.

Dynamically Averaged *J*-Couplings. The dynamically averaged *J*-couplings were calculated using the Karplus equations[44,45] for nucleic acids.[41,52−55] The three-bond ^3J-couplings were mostly assigned to the corresponding torsion angles. Since several variants of the Karplus equations are available for the individual torsion angles (three for β and ε, five for γ and δ) and there is no consensus on which of them is to be preferred, we used their average as reported in the Supporting Information instead. For the two-bond couplings ^2J(C3′1,P) and ^2J(P,C5′2) assigned to the ζ1 and α2 torsionss, respectively, we used the theoretical model based on our previous calculations[46] (the model correlates three intervals of 0−120°, 120−240°, and 240−360° for the ζ1 and α2 torsions with the values of −7.1, −4.9, −7.1 Hz and −6.1, −3.3, −6.1 Hz, respectively). The glycosidic torsion χ was determined with the Karplus equation parametrized theoretically for the ^3J(H1′,C) couplings by Munzarová and Sklenář[55] and Wijmenga.[41] The dynamically averaged *J*-couplings were calculated as numerically integrated Karplus equations with a distribution function of the respective torsion angle ($J = \sum_{i=1,...,36} J(\tau_i)\cdot n_i$, where $J(\tau_i)$ is the middle value of the Karplus equation in the *i*th subinterval and n_i is the value of the normalized distribution for torsion τ).

Results and Discussion

Selection of the Initial Structures for the MD Calculation. ***Short RNA Molecules in the Solid State.*** RNA molecules containing cytosine and/or adenine (labeled jointly as "C/A" here in this section) were queried in the Nucleic Acid Database (NDB[56]) and compared to the consensus RNA conformers as defined by Richardson et al.[57] Of the six such C/A dinucleotide structures available in the NDB (ApA: urb003, drb002, ApC: urb001, CpA: drb005, drd004, CpC: udbs38; see Figure 1), two are structures of uncomplexed ribonucleotides (urb003, urb001), but only urb003 has a standard 3′−5′ phosphodiester link; the backbone in urb001 contains a 2′−5′ link. Three of the dinucleotide structures are C/A complexes with the intercalating drug proflavin (drb002, drb005, drd004), and one contains chemically modified deoxyribose and forms a parallel minihelix. Also, trinucleotide RNA structures are rare in the NDB; in fact, only one uncomplexed trinucleotide ApApA (urc002) has been deposited, and no C/A RNA tetranucleotide was found.

All of the above-mentioned structures are well-resolved crystal structures providing reliable information about their molecular conformations, but the number of these structures is rather limited and does not allow for a statistical analysis of the observed features. We, therefore, decided to search for short RNA fragments cocrystallized with other RNA and/or proteins in protein/RNA complexes. Approximately 10 such structures were found, including, for instance, the complex between ribonuclease PARN and trinucleotide AAA (pr0068), C_3 and C_6 oligonucleotides in a complex with a transcription termination factor RHO (pr0008), and several complexes between ribosomal particles and short RNA, such as A_4 mimicking mRNA in a small ribosomal subunit (rr0096) or CCA as an analogue of the 3′ end of the deacylated tRNA in a large ribosomal subunit (rr0049). These RNA fragments extended the analysis, but the quality of this data is limited by low resolution while their number (less than 30 C/A steps altogether) would still not allow a rigorous statistical analysis of the conformational behavior of the C/A step in RNA single-stranded stretches of two to four nucleotides.

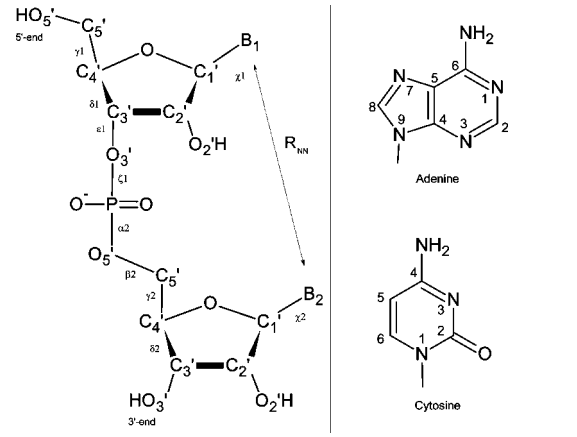

Figure 1. A chemical diagram of the B_1pB_2 DMP molecule (ApA, CpA, ApC, CpC). B_1, B_2 is an adenine or cytosine base of the 5′-B_1pB_2-3′ DMP molecule. R_{NN} is the distance between the nitrogen atoms of the bases involved in the glycosidic bond (N1 of C, N9 of A). Indexes "1" and "2" refer to the geometry parameters of the 5′- and 3′-nucleoside; γ1 = O5′1−C5′1−C4′1−C3′1, δ1 = C5′1−C4′1−C3′1−O3′1, ε1 = C4′1−C3′1−O3′1−P, ζ1 = C3′1−O3′1−P−O5′2, α2 = O3′1−P−O5′2−C5′2, β2 = P−O5′2−C5′2−C4′2, γ2 = O5′2−C5′2−C4′2−C3′2, δ2 = C5′2−C4′2−C3′2−O3′2, χ = O4′−C1′−N1−C2 (cytosine), χ = O4′−C1′−N9−C4 (adenosine).

TABLE 1: The Values of the Torsion Angles in Degrees Averaged for the RNA Structural Classes Populated in the Ribosomal RNA[58] Selected As the Initial Structures in the MD Calculations[a]

class[b]	class[c]	γ1	δ1	ϵ1	ζ1	α2	β2	γ2	δ2	χ1	χ2
1a	20	54	81	211	291	296	175	54	84	198	202
1c	19	53	81	194	292	156	194	180	83	203	298
3d	15	53	81	225	211	60	201	49	81	198	196
#a	7	156	149	195	150	292	147	46	84	257	185
6d	9	294	148	237	83	68	175	58	149	56	240

[a] These structures were taken as the starting geometries in the MD simulations. [b] New notation used in this work by Richardson et al.[57] [c] Old notation used in our previous work,[46] numbering according to Table 3 in ref. [58]

Despite the relative lack of data, we can draw a qualitative conclusion that the analyzed short single-stranded RNAs containing C and A nucleotides exhibit a high conformational variability. These molecules can acquire conformations from the canonical A-RNA form as the first AA step in urc002, but a variety of other conformers are also populated. Some can be characterized as a deformed A-form, as in the "crankshaft" conformation AII, which is labeled also as consensus conformer 1c (Table 1, Figure 2); other conformations have one sugar pucker C2′-*endo* rather than the usual C3′-*endo*, leading to a relatively mildly deformed A-form as in the CA step of drb005 (consensus class 1b). There are also more deformed conformations of the second AA step of urc002 which are close to the consensus class 5z locally resembling a Z-DNA form. Two ApA

Figure 2. A stereoview overlay of the ApA dinucleoside monophosphate (NDB entry urb003) (black) and the structural class 6d (gray).

dinucleosides, the "naked" urb003 and the proflavine complex drb002, have open and unstacked conformations, while AA in urb003 is close to the class 6d. The conformations of the AA steps found in the complexes with proteins are mostly close to a helical conformation (pr0166, rr0096, pr0068); also, the CCA sequence in the structures of the rRNA subunit (e.g., rr0049) has an almost helical conformation. On the other hand, the CAUC sequence (the NMR structure of the 2i2y fusion protein/RNA complex) is nonstacked with an almost zero rise of bases ("platform" conformers such as #a).

An Ensemble of the Initial Structures for the MD Calculations. The large flexibility of short single-strand RNAs, their open conformations with nonstacked bases, and dissimilarity to the canonical A-RNA form suggest that the conformational space of these molecules should be sampled more comprehensibly. The initial structures for the MD calculations should thus include, besides the canonical A-form, at least some of the noncanonical conformers. Therefore, for each sequence, we considered five different starting structures, corresponding to RNA families 1a, 1c, 3d, #a, and 6d (Table 1). The geometries of these conformers were taken from a previous study.[58] Families 1a and 1c represent the major and minor A-RNA backbone conformations, known also as AI and AII;[59] #a can be characterized as a platform with a zero rise of bases, and the conformer 3d has unstacked, entirely separated bases; the conformer occurs at the beginnings and ends of the double helices. The use of these five different conformers as the starting structures greatly enhances the sampling of the MD simulations since they cover a variation of all of the important structural features of the backbone angles, base-stacking arrangements, and sugar pucker. We are obviously far from claiming that our five 50 ns simulations for each DMP sequence (20 simulations in total) guarantee convergence of the results. Nevertheless, as shown below, we suggest that our simulation time scale provides enough sampling to achieve a qualitatively meaningful population of the key backbone torsion angles that is sufficient for comparison with the experimental data.

An Analysis of the Molecular Dynamic Calculation. The analysis of trajectories makes it possible to suggest several conclusions. The dynamics calculated for the different torsions occur on specific time scales and possess characteristic torsion angle amplitudes (by amplitude of torsion, we mean here the confined interval of the torsion angle values substantially populated for a given torsion, thus giving rise to a separate peak of the corresponding distribution). For example, the oscillations between the characteristic amplitudes of the torsion angles α, γ, and ζ occur on a scale of tens of ns, whereas in the case of the δ torsion, the time scale of the flips is around 1 ns. The amplitudes for the χ torsion are broader than those calculated for the α, γ, and ζ backbone torsions, despite their flips among their typical amplitudes occurring on a similar time scale. The specificity of the motions calculated for the structural parameters of the DMP molecules is large. The following discussion is thus focused on the local dynamics of the torsion angles, including their mutual correlations, and on the characterization of the individual distribution functions used for correlating the calculated *J*-couplings with the NMR experiment. The global structural features like the stacking of bases and their relation to various backbone topologies are discussed separately below.

For the sake of clarity, we have named each simulation in the following way. The simulation with the starting structure N (as indicated in Table 1) of the XpY sequence will be further referred to as NXpY. Thus, for example, Figure 3 shows the full time development and distribution for the #aCpC simulation. All of the other trajectories and distributions can be found in the Supporting Information.

An analysis of the $\alpha 2$, $\gamma 2$, and $\zeta 1$ torsion angles unveils their strong mutual correlation manifested as concerted flips between their typical amplitudes. Each of the three torsion angles has, in principle, a trimodal distribution (g+ (60°), t (180°), g− (300°)), but only certain combinations of their amplitudes were populated. The $\alpha 2$/g−, $\gamma 2$/g+, $\zeta 1$/g− triad that pertains to A-RNA (class 1a, i.e. the canonical A-RNA, Table 1) was populated for 52% of the total simulation time, and the second most populated triad $\alpha 2$/g+, $\gamma 2$/t, $\zeta 1$/g+ was seen for ∼19% of the simulation time. Other triads had a fast oscillatory character, and their overall residence time was shorter; they were seen for less than 10% of the total simulation time (Figure 5). The results are in qualitative agreement with the simulations of A-RNA as well as folded RNAs. Specifically, A-RNA simulations with the same force field show the dominance of the canonical g+/g− for α/g and a ∼10−15% population of the short-living (0.1−20 ns) g+/t substates.[60,61] The crystal structures of the RNA oligonucleotides indicate ∼5% population of g+/t for α/γ. Therefore, the α/γ clearly represent an intrinsic feature of the RNA backbone.[58,60,61]

The concerted flips of the amplitudes calculated for the $\alpha 2$, $\gamma 2$, and $\zeta 1$ torsions either occur coherently ($\alpha 2$/g−, $\gamma 2$/g+, $\zeta 1$/g− → $\alpha 2$/g+, $\gamma 2$/t, $\zeta 1$/g+, #aApA) or may include only a subgroup of the torsions ($\alpha 2$/g−, $\gamma 2$/t, $\zeta 1$/g− → $\alpha 2$/g−, $\gamma 2$/g+, $\zeta 1$/g− → $\alpha 2$/g+, $\gamma 2$/t, $\zeta 1$/g+; 1cApC simulation). Flips in the $\alpha 2$, $\gamma 2$, or $\alpha 2$, $\zeta 1$ subgroup of torsions were rather frequent, whereas the flip of the $\gamma 2$, $\zeta 1$ torsions were always accompanied with a flip of the $\alpha 2$ torsion. This may imply that concerted oscillations in the $\zeta 1-\alpha 2-\gamma 2$ segment include primarily the $\alpha 2$ torsion (via $\alpha 2 \leftrightarrow \gamma 2$ and/or $\alpha 2 \leftrightarrow \zeta 1$ coupling), while isolated oscillations in the $\zeta 1-\gamma 2$ subsegment are not allowed.

The $\alpha 2$/t and $\zeta 1$/t amplitudes were not populated at all, in agreement with the X-ray data.[58] Whenever the $\gamma 2$/t amplitude appeared in a trajectory, both $\zeta 1$ and $\alpha 2$ torsions adopted either g+ or g− orientation. The 5′-hydroxyl undergoes a relatively free rotation, and the $\gamma 1$ trajectories show faster oscillations between the $\gamma 1$/g+ and $\gamma 1$/t amplitudes than the trajectories of the $\gamma 2$ torsion.

Allow us now to comment on the influence of the initial structures on the sampling. Although the simulations of each DMP were started assuming five different geometries and we generally did see quite many transitions, the influence of the starting structures is visible. The MD calculations with the initial class 1a geometry (canonical A-RNA) retain mostly the initial

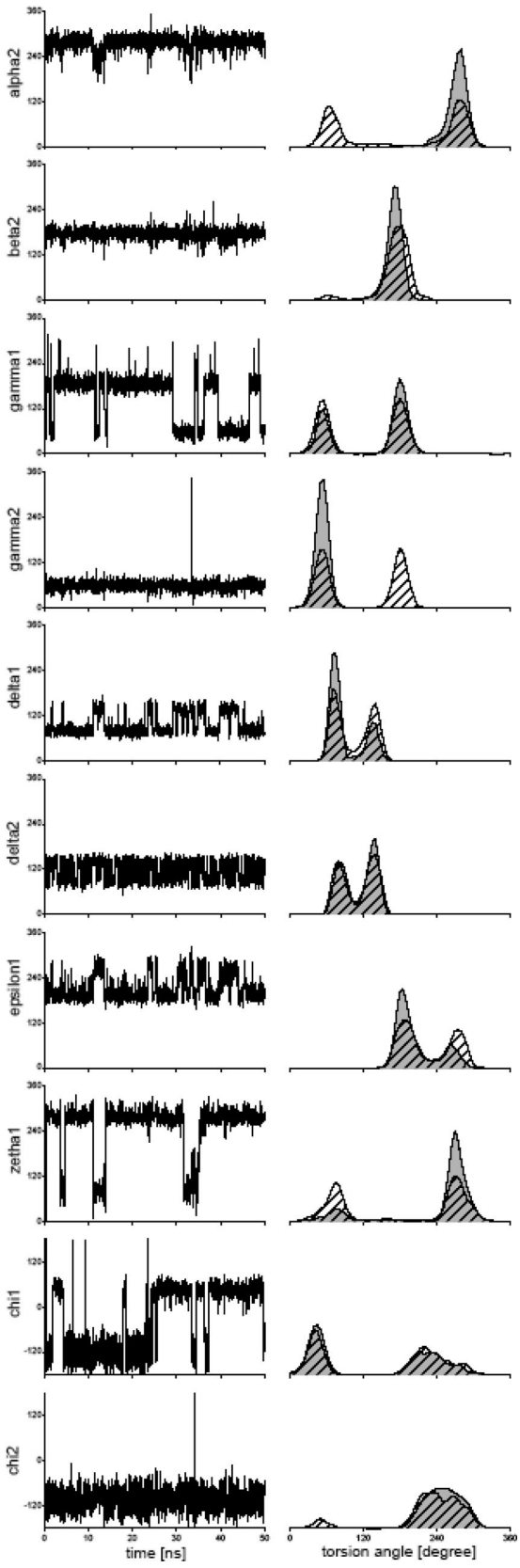

Figure 3. The evolution of the torsion angles over 50 ns and their probability distribution functions for the #aCpC DMP calculated for the temperatures 300 (gray) and 340 K (shaded). The complete data for all of the simulations are in the Supporting Information.

α2/g− and γ2/g+ amplitudes as compared to the stability of those calculated with class 1c, differing only in the α2/t and γ2/t amplitudes (Table 1, Figure 5). The γ2/t amplitude was

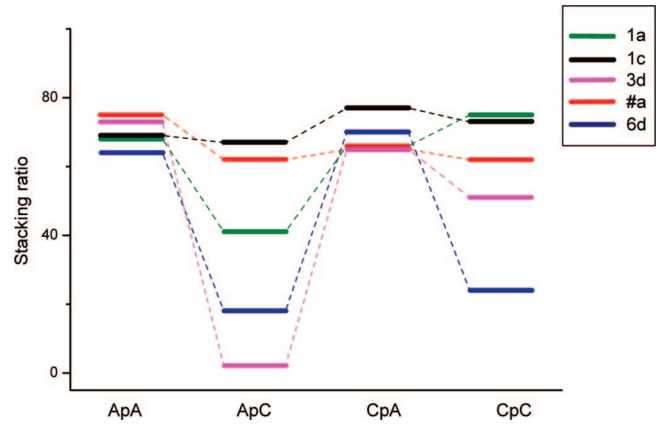

Figure 4. The dependence of the calculated base-stacking ratio (percentage of the geometries with bases in a stack in the course of the simulations) on the sequence of the RNA dinucleoside monophospates calculated with the five initial structures (inset top right; cf. also Table 2).

populated significantly only in the 1cCpA calculation, a mixture of the γ2/t,g+ was found in the 1cApC trajectory, while the 1cApA and 1cCpC trajectories were dominated by the γ2/g+ amplitude. This fact may indicate a preference for the canonical A-RNA pattern. The overall tendency for convergence toward the α2/g−, γ2/g+ pattern of A-RNA was not observed because in some calculations with different starting structures lasting 50 ns, it was not populated (Figure 5). The initial RNA backbone patterns (Table 1) selected from their complete ensemble[57] thus represent reliable energy minima with a high individual potential to be populated.

The ε1 torsion angle basically oscillates between the ∼180 and ∼260° amplitudes, except for rare and short-lived populations with an ε1 of ∼ 60° (6dCpA, 1aApA). The fast oscillations of the ε1 torsion (6d-ApC,CpC) are sometimes damped (1cCpA), and if so, one of the dominant amplitudes is populated more. The coherent oscillations of the ε1 and δ1 torsions calculated for the 1cXpY, X,Y = A,C, DMP molecules may indicate their possible coupling, and the higher population of ε1 ∼ 260° may thus be correlated with the stabilization of the C2′-*endo* ribose (1cCpA).

The single β2/t amplitude was calculated to be overall dominant in all 20 simulations.

The calculated flexibility of the ribose sugar is large, and oscillations between the C2′- and C3′-*endo* ribose conformers can be related to the δ torsion amplitudes of ∼140 and ∼80°, respectively. The local motions of riboses at the 3′ and 5′ end are not equivalent. The oscillations calculated for the δ2 torsion are harmonic, whereas the motion of ribose at the 5′ end seems to be perturbed by a rotating 5′-hydroxyl. Neither the C2′- nor the C3′-*endo* conformer was thus calculated as dominant in nucleotides at the 3′ end of the DMP molecules. On the other hand, the calculated overall motion of ribose at the 5′ end was stabilized either in the C2′-*endo* (3dCpC, 1cCpA) or C3′-*endo* (#aCpC, 1cCpC, 1aCpA,CpC) conformation.

The distribution functions calculated for the glycosidic χ torsion have two maxima at ∼60 and ∼240°, corresponding to the *syn* and *anti* sugar-to-base orientations in RNA nucleosides. The χ2/*anti* conformer appearing in all of the initial structures was also calculated as being overall dominant. The average value of the χ2/*anti* amplitude calculated in the ApA and CpA (χ2 ∼ 280°) is larger than that calculated in the ApC and CpC (χ2 ∼ 250°) molecules. The mean value of the χ2/*anti* distributions thus specifically depends on the nucleobase type. The χ1 torsion

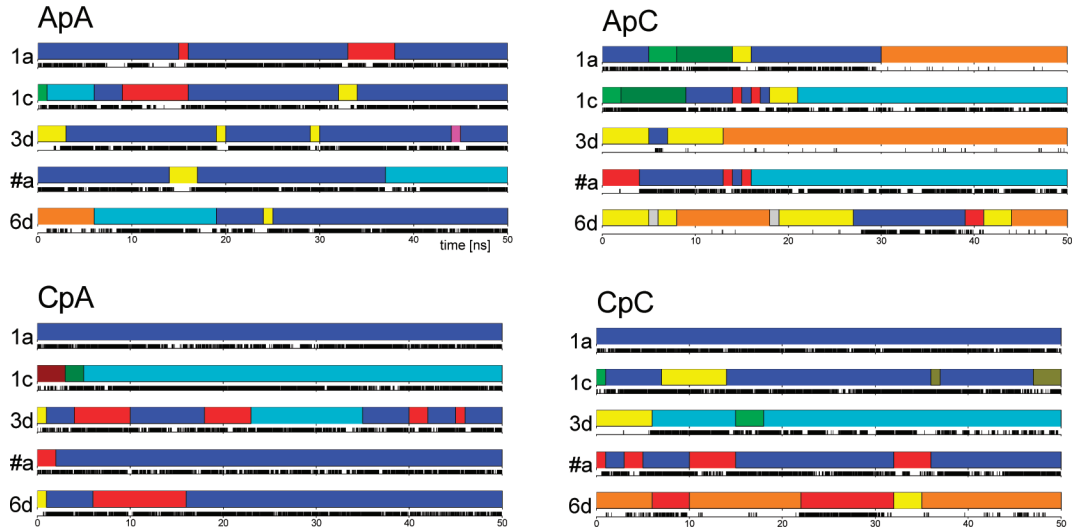

Figure 5. The correlation between the geometry of backbone segment α2, γ2, ζ1 (upper stripe) and base stacking (lower stripe, with the color black corresponding to the geometries with stacked bases) during the time evolution calculated for the 1a, 1c, 3d, #a, and 6d initial patterns of RNA molecules. The values of the torsion angles α2/ γ2/ ζ1 in degrees and the calculated percentage of their populations are 300/60/300 (52%, blue), 60/180/60 (19%, cyan), 60−180/60/60 (11%, orange), 60/60/60 (6%, yellow), 300/60/60 (8%, red), 300/180/300 (2%, olive), 60/180/300 (1%, green), 60/60/300 (1%, dark yellow), 60−180/180/300 (1%, wine), 60/60/180 (1%, light gray), and 300/60/180 (1%, magenta).

undergoes frequent flips between the *syn* and *anti* orientations, and the χ1/*syn* orientations were calculated as being overall dominant. Interestingly, the *syn* and *anti* regions of the χ1 distributions for the ApA and ApC are smoothly jointed (via point χ1 ∼ 360°), unlike the separated regions calculated for the CpA and CpC molecules. The flexibility of the glycosidic bond calculated for the nucleoside at the 5′ end, which is specific for adenosine and cytidine, can be again most likely attributed to the steric interactions of the 5′-hydroxyl with the nucleobases.

An Analysis of Base Stacking. The base stacking interaction plays an essential role in stabilizing the structure of nucleic acids. The model RNA molecules containing permutations of purine and pyrimidine nucleobases were synthesized to this end. They represent the simplest but still relevant models for a sequential study of base stacking in short single-strand RNA molecules.

The mutual geometrical arrangement of the nucleobases was classified according to the following criteria: the distance R_{NN} (Figure 1) between the glycosidic nitrogen atoms of the nucleobases (with these distances observed in the MD simulations being in the range of 3.3−12.0 Å), the ϕ angle between the in-plane vectors in the adenine (N9 → C6) and cytosine (N1 →C4) bases, and the ϕ angle between the bases' normal vectors. Similar geometry criteria were used for the base-stacking analysis of the nucleic acid macromolecules.[62] In this work, the mutual inclination of the planes defined by the inner-ring atoms of nucleobases was thus measured with the two angles (the angular geometry criteria), while their proximity was probed with the R_{NN} distance. The DMP molecules with a geometry having an $R_{NN} \leq 6.4$ Å, $\phi \leq 60°$, and $|\phi| \leq 45°$ (parallel bases) or $|\phi| \geq 135°$ (antiparallel bases) were classified in this work as the DMP molecules with an arrangement of stacked bases. An evaluation of the base stacking was thus grounded purely on the complex geometry criteria selected to capture roughly the maximal spatial overlap of bases in the DMP molecules (for the time evolution of the three geometry parameters, see the Supporting Information). The base-stacking ratio was evaluated as the number of snapshots having a geometry corresponding to stacked bases relative to the total number of snapshots accumulated along a given trajectory (Figure 4).

The calculated base-stacking ratios depended on the starting MD structures. This ratio was for the ApC and CpC molecule in the ranges of 2−67 and 24−75%, respectively (Figure 4). The ApC and CpC simulations with the 1a and 1c initial geometries show high stacking ratios (67, 41% and 73, 75%, respectively). In these two molecules, the angular part of the geometry criteria for base-stacking classification provided more reliable measure of the stacking ratio, elsewhere frequently off the range, while the R_{NN} distance simultaneously fit the criteria for stacked bases.

The maximal base-stacking population was calculated consistently (for all five initial structures) for the ApA (64−75%) and CpA (65−77%) molecules (Figure 4). For both of these DMPs, the distance geometry criteria R_{NN} turned out to be decisive since the angular criteria appeared mostly within the target intervals. Adenosine at the 3′ end of the DMP molecules thus stabilizes the stacked conformations, regardless of the nucleobase at the 5′ end. The same conclusion had been drawn by Norberg and Nillson as well.[49]

The Relation between the Conformation of the RNA Backbone and Base Stacking. The motions calculated for the backbone torsion angles in the DMP molecules can be roughly classified as constant (the behavior of angle β), oscillating among well-resolved amplitudes with a frequency of tens of ns (α, γ, ζ, and ε torsions) and oscillating fast on the nanosecond time scale between well-resolved amplitudes (δ torsion). The analysis of the conjoint motions in the RNA backbone and nucleobases thus primarily focused on the semirigid segment ζ1−α2−γ2.

The simultaneous population of the dominant triad/angle combination α2/g−, γ2/g+, ζ1/g− (canonical A-RNA) and the bases in stack geometry was found 72% of the time when this triad was populated. The α2/g+, γ2/t, ζ1/g+ triad ranked the second most consistent with base stacking, similarly with 68%. The populations calculated for the rest of the α2, γ2, ζ1 triads found in the MD trajectories decreased steeply, and their coherence with the base stacking was therefore overall negligible (Figure 5).

The base-stacking topology in the DMP molecules was found not only for the canonical A-RNA backbone pattern of the

TABLE 2: The Scalar Coupling Constants in Hertz Measured and Calculated in the ApA, ApC, CpA, and CpC Molecules and Their Structural Assignment

			J(HH)			*J*(H,P)			*J*(C,P)				*J*(H,C)	
			3′,4′	4′,5′	4′,5″	3′,P	5′,P	5″,P	2′,P	3′,P[b]	4′,P	5′,P[b]	1′,2/4	1′,6/8
compound		unit[a]	$\delta1/\delta2$	$\gamma1/\gamma2$	$\gamma1/\gamma2$	$\varepsilon1$	$\beta2$	$\beta2$	$\varepsilon1$	$\zeta1$	$\epsilon1/\beta2$	$\alpha2$	$\chi1/\chi2$	$\chi1/\chi2$
ApA	exp.[c]	A	~5.0	2.5	3.6	~9.0			3.7	−5.4	5.3		1.9	4.2
		A	5.5	?	~3.8		?	~3.8			9.4	−5.4	2.5	3.1
	calc.[c]	A	4.0	2.4	4.9	7.2			4.5	−5.3	4.9		3.4	3.1
		A	2.8	2.1	3.2		4.2	2.3			9.6	−4.7	2.7	2.9
ApC	exp.[c]	A	6.1	2.4	3.5	8.7			3.3	−5.3	4.6		2.1	2.8
		C	?	~1.7	~2.0		~4.0	3.4			9.5	−5.1	1.4	4.5
	calc.[c]	A	6.0	2. 5	4.3	5.6			3.6	−5.2	6.6		3.8	2.6
		C	3.8	2.2	4.4		2.8	3.9			9.6	−4.4	3.1	3.1
CpA	exp.[c]	C	6.8	2.6	4.0	8.7			3.4	−5.3	5.4		1.6	4.6
		A	5.5	2.6	3.0		4.3	3.8			9.3	−5.3	1.8	4.3
	calc.[c]	C	5.5	2.3	5.1	6.5			4.4	−5.3	5.4		3.3	4.0
		A	3.7	2.2	3.9		2.9	3.0			10.0	−4.7	2.6	3.5
CpC	exp.[c]	C	7.3	2.5	3.8	8.9			3.1	−5.3	6.0		1.4	4.5
		C	7.2	2.4	2.4		4.3	3.2			9.5	−5.6	1.4	4.6
	calc.[c]	C	6.4	2.3	6.0	5.6			3.2	−5.3	7.0		4.3	4.1
		C	4.5	2.3	3.4		2.9	3.0			10.0	−4.7	3.4	3.6
	exp.[d]	C	6.7	2.6	4.0	8.7			3.4	−5.3	5.5		1.7	4.6
		C	6.7	~2.5	2.7	~4.3	3.9				9.1	−5.3	1.5	4.6
	calc.[d]	C	6.0	2.3	5.3	6.1			3.6	−5.2	6.3		3.7	4.0
		C	4.4	2.3	4.3	3.2	3.5				9.6	−4.6	3.1	3.6

[a] The upper and lower rows show the data for the nucleoside at the 5′ and 3′ end of the RNA dinucleoside, respectively. [b] The negative sign was calculated previously.[46] [c] At a temperature of 300 K. [d] At an experimental temperature of 320 K. The MD simulation at 340 K. The values were calculated only with the distributions obtained for the 1c and #a structural classes.

$\zeta1-\alpha2-\gamma2$ segment but also for other patterns (Figure 5). The sequential role of purine or pyrimidine nucleobases at the 3′ end of the DMP molecule discussed in the previous chapter is also critical (Figure 4). The calculations for the ApA and CpA molecules with overall high stacking ratios as well as those for the other two RNA molecules exhibited a large portion of the antiparallel arrangement of stacked bases (see the Supporting Information). Since the nucleosides at the 3′ end fluctuate fairly well around the *anti* orientation of their glycosidic bond, the main reason for the antiparallel orientation of the stacked bases is a rather high population of *syn* nucleosides at the 5′ end of the DMP molecules (see the Supporting Information). The analysis of the *J*-couplings assigned to the glycosidic torsion in adenosines (the following section) also supported the calculated prevalent population of the *anti* and *syn* adenosine at the 3′ and 5′ end, respectively.

The Structural Assignment and Calculation of the *J*-Couplings. The geometry descriptors that were used for calculating the structure of the DMP molecules are eight backbone torsion angles (two of which are correlated with the sugar pucker) and two glycosidic torsion angles (Figure 1). The *J*-couplings across the three covalent bonds (the ^3J-couplings) were assigned to the majority of the torsion angles.[41,46,54,55] The ^2J-couplings near the phosphate group were assigned to the α and ζ torsion angles (see Methods Section).

The accuracy of the ideally smooth empirical dependencies for the ^3J-couplings (Karplus equations) is limited. For example, several Karplus equations designed for one *J*-coupling may differ despite their phase factor usually remaining the same.[41] Some examples of such Karplus equations were collected in our previous work (see Figure 2 of ref 46 and the references therein). Also, the one-dimensional character of the Karplus equations cannot always be guaranteed, but the effect of the neighboring geometry can be modeled.[46,63] The absolute accuracy of the calculated *J*-couplings can thus be analyzed carefully, taking into account the mentioned facts. Being conscious of the limitations, the theoretical method applied in this work can be used for directly probing the local geometry with NMR spectroscopy parameters.

The ^3J(P, H5′2), ^3J(P, H5″2), and ^3J(P,C4′2) couplings were assigned to the $\beta2$ torsion.[41,46] The three Karplus equations possess different phases with respect to the calculated distribution functions centered near 180°. The dispersion of the values measured for each of the three *J*-couplings in the DMP molecules is smaller than 0.6 Hz, although their individual magnitudes are different (Table 2). This fact along with the different phase factors of the three *J*-couplings implies that the $\beta2$ torsion should be similar in all four DMP molecules. The actual distribution function should be correspondingly single-modal, in agreement with the calculated distributions, which are centered near 180°. The absolute difference between the calculated couplings assigned to $\beta2$ torsion and experiment was smaller than 1.5 Hz.

Interestingly, the dependence of the averaged *J*-couplings on the curvature and exact position of the central point of the $\beta2$ distributions is large. Specifically, the center of the $\beta2$ distribution for the ApA molecule is at 172° and has a slightly wider envelope than the distribution calculated for the ApC molecule centered at 179° (see the Supporting Information). The ^3J(P,C4′2) couplings calculated in the ApA and ApC molecules are practically the same because the $\beta2$ distribution and Karplus equation are "in phase", both centered near 180° (for an example of the Karplus equations, see Figure 2 in ref 46). On the other hand, the ^3J(P, H5′2) and ^3J(P, H5″2) couplings calculated in the ApA and ApC molecules differ by 1.4 and 1.5 Hz, respectively. Their Karplus equations are not centered at 180°, and their slopes have opposite declination in that area. The mutual phase of the Karplus equation and the corresponding distribution may thus become a very sensitive factor in the numerical averaging of *J*-couplings.

The ^3J(H3′,H4′) coupling assigned to the δ torsion was used to calculate the sugar pucker. Its extreme values roughly ranged

from 0 (C2′-*endo*) to 10 Hz (C3′-*endo*) (see Figure 2 in ref 46). The measured values between 5.0 and 7.3 Hz suggest the presence of a mixture of the two conformers. Thus, a more equal population of the C2′- and C3′-*endo* pucker was measured in the ApA, whereas in the CpC molecule, the C2′-*endo* sugar dominated. The measured trends were also calculated, although the calculated values of the ^3J(H3′,H4′) couplings are overall underestimated.

The ^3J(H4′,H5′) and ^3J(H4′,H5″) couplings assigned to the γ torsion with a trimodal pattern of 60,180, 300° have approximate magnitudes of 3, 3, 10 Hz and 3, 10, 3 Hz, respectively.[41] Better overall agreement was obtained for the ^3J(H4′,H5′) coupling, with an absolute deviation of the calculated couplings from experiment that was smaller than 0.5 Hz. Systematically larger deviations from experiment (up to 2.4 Hz) were calculated for the ^3J(H4′,H5″) coupling. The calculated γ1 distributions show populations of its trans conformer, although g+ is expected to be dominant at least in the solid phase.[58] Any conclusion in that regard can be drawn only with difficulty because of the limits in accuracy as the γ1 distributions are very narrow, which causes the numerical integration method to probe only a very confined interval of the respective Karplus equation.

The ^3J(C2′1,P), ^3J(C4′1,P), and ^3J(H3′1,P) couplings were assigned to the ε1 torsion.[41,46] The two calculated ^3J(C,P) couplings deviated from the experiment by less than 1 Hz (except for the ^3J(C4′1,P) coupling in the ApC molecule), while the deviations calculated for the ^3J(H3′1,P) coupling ranged from 1.8 to 3.3 Hz.

The assignment of the ^2J(P, C5′2) and ^2J(C3′1,P) couplings to the α2 and ζ1 torsion is a challenging part of this work since the dependence of the ^2J-couplings on the torsion angles is less straightforward than that for the ^3J-couplings. On the other hand, the ζ1−α2 backbone segment suffers from a lack of relevant nuclei measurable by means of NMR spectroscopy. The two couplings therefore offer one of the limited possibilities for probing the structure of the nucleic acids near the phosphate group, as calculated previously.[46] The proposed dependence of the ^2J-couplings on the ζ1 and α2 torsions seems to be qualitatively correct since it does not contradict the experimental data.

The ^3J(H1′,C2/4) and ^3J(H1′,C6/8) couplings were assigned to the χ torsion.[55,64] The values of the *J*-couplings calculated by Munzarová and Sklenář for the *syn*/*anti* nucleosides are 5.5/2.5 Hz for both the ^3J(H1′,C4) coupling in adenosine and the ^3J(H1′,C2) coupling in cytidine, 4.0/5.0 Hz for the ^3J(H1′,C8) coupling in adenosine, and 5.5/4.5 Hz for the ^3J(H1′,C6) coupling in cytidine.[64] The *syn* and *anti* regions of both dependencies used for the determination of the χ torsion actually coincided with the two maxima on the Karplus curves.[41,64]

The ^3J(H1′,C8) couplings measured in the different adenosines have different values, namely, ApA (4.2, 3.1 Hz), ApC (2.8 Hz), and CpA (4.3 Hz). A similar variation was also measured also for the ^3J(H1′,C4) couplings (see Table 2). On the contrary, both couplings assigned to the χ torsion measured in cytidines varied by less than 0.2 Hz.

The calculated χ distributions are sequence-dependent. The χ1 and χ2 distributions both have a similar shape, irrespective of the nucleobases. Specifically, the χ1 distributions possess a sharp *syn* peak as compared to the χ2 distributions, and χ2 distributions have a broad *anti* peak; this, however, contradicts the experimental data. The ^3J(H1′,C2) and ^3J(H1′,C6) couplings measured in cytidines have practically the same values, while the calculated ones were modulated by the specificity of the χ1, χ2 distributions (Table 2). This discrepancy can be most likely attributed to the drawbacks of the force field used.

The ^3J(H1′,C2) couplings measured in cytidines (∼1.5 Hz) are certainly below the proposed *syn* (5.5 Hz) and *anti* (2.5 Hz) magnitudes.[64] Therefore, glycosidic motion in all cytidines should be rather uniform and delocalized, probably corresponding to the broad distribution that is dominant in the *anti* region.

The increase of the ^3J(H1′,C8) coupling and simultaneous decrease of the ^3J(H1′,C4) coupling as measured in adenosines can be assigned to the increase of the *anti* population and vice versa.[55,64] (The global maxima of the dependencies calculated for the two *J*-couplings swap; ^3J(H1′,C8)/*syn* < ^3J(H1′,C8)/*anti* and ^3J(H1′,C4)/*syn* > ^3J(H1′,C4)/*anti*.) The *anti* population of the 3′-adenosine in the ApA molecule should thus be higher than the *anti* population of the 5′-adenosine. Similarly, the *syn* population of adenosine in the ApC should be higher than the *syn* population of adenosine in the CpA molecule. We note that this site-specific assignment for the glycosidic torsion of adenosines in the DMP molecules is in agreement with the calculated stacking ratios (see Figure 4). The absolute deviation of the calculated *J*-couplings assigned to the χ torsion in adenosines from the experiment ranged up to 1.7 Hz.

***J*-Couplings for the CpC Molecule at a Temperature of 340 K.** The MD calculations at a temperature of 340 K were carried out only for the CpC molecule with the 1c and #a initial structure (see the Supporting Information). The dynamics of the CpC molecule at the higher temperature possess more frequent oscillations of the torsion angles accompanied with a decrease of the base-stacking ratio from 62 to 46% for the #aCpC calculation and from 73 to 57% for the 1cCpC calculation. A similar drop in the base-stacking ratio had previously been calculated in the ApA dinucleoside by Norberg.[65] The calculated distributions are quite strongly modulated by temperature increase (Figure 3).

The absolute shift of the measured *J*-couplings with the temperature increase was smaller than 0.7 Hz as measured for the ^3J(P, H5″2) coupling assigned to the β2 torsion. The decrease of the ^3J(H3′,H4′) coupling by 0.5 Hz measured in both cytidines can be assigned to the more equal populations of the C2′- and C3′-*endo* sugar pucker conformers when compared to the populations at lower temperature (Table 2). (The equilibrium can be estimated for the *J*-coupling magnitude of ∼5 Hz.).

The faster molecular motions calculated for the backbone atoms related to the torsion angles modulate the shape of the calculated distributions (Figure 3). The *J*-couplings calculated at the higher temperature assigned to the backbone torsions mostly follow the measured trends, except for the ^3J(H3′1,P) and ^3J(P, H5′2) couplings (Table 2). The absolute temperature shift of the calculated *J*-couplings was smaller than 0.9 Hz. Interestingly, the temperature shift calculated for the *J*-couplings assigned to the glycosidic torsion ranged from 0.3 to 1.5 Hz. This fact again pointed to possible deficiencies in the dynamics calculated for the glycosidic motions and to the fact that a higher overall reliability should be attributed to the results obtained for the backbone torsion angles.

Conclusion

The NMR scalar *J*-coupling constants measured in the ApA, ApC, CpA, and CpC RNA dinucleoside monophosphates were assigned to the α, β, γ, δ, ε, and ζ backbone torsion angles and to the χ glycosidic torsion. Assembling the local structural information for the individual torsion angles that had been validated with the NMR *J*-couplings allows for the determination

of the individual global structural and dynamical features of the RNA molecules.

The measured scalar *J*-couplings were correlated with the *J*-couplings calculated using the Karplus equations averaged with the distributions for the torsion angles obtained from the MD simulations. The sampling of the structural patterns in the MD calculations was enhanced by taking the initial patterns populated in rRNA resolved in the solid state into account.[57,58] The calculation method can thus reliably and consistently probe the dynamical multiamplitude character of the torsion angles and their relative populations with NMR spectroscopy.

Overall, good agreement of the measured and calculated *J*-couplings was obtained particularly for the backbone torsions. The absolute average deviation from experiment was 0.4, 0.6, 1.6, 1.0, and 1.1 Hz for the ^2J(P,C)/(α,ζ), ^3J(P,C)/(ε,β), ^3J(P,H)/(ε,β), ^3J(H,H)/(δ,γ), and ^{3}J(C,H)/(χ) couplings. For the calculation of the α and ζ torsions, the ^2J(P,C) scalar couplings were newly used. The calculated scalar *J*-couplings assigned to the glycosidic torsion contradict the measured data, most likely because of the possible drawbacks of the force field used, which probably failed in the qualitative prediction of this large-amplitude motion in the nucleosides of the four RNA molecules. In that respect, a better robustness of the calculation method should be expected for the relatively rigid geometry as calculated for the RNA backbone. However, the "static assignment" of the experimental *J*-couplings across the glycosidic torsion (i.e., the direct relation of the measured *J*-couplings to the χ torsion angles via Karplus curves without introducing the distributions for torsion angles) implied different dynamics in cytidines (steady motion) and adenosines (sequence-specific motion) in the DMP molecules.

The magnitudes of the calculated *J*-couplings depend critically on the distribution functions of the torsion angles. Another critical parameter is the mutual symmetry of the distribution and Karplus equation, as was shown for the three ^3J-couplings assigned to the β torsion.

The set of distribution functions for the torsion angles, which is coherent with the structural pattern of A-RNA, was overall resolved as the most populated. Specifically, the distributions calculated for the α2, γ2, ζ1 torsion angles with the pattern of A-RNA dominate overall, and such geometries enhance the stacking of the bases in the RNA dinucleoside monophosphates. Further, an important prerequisite for the base-stacking topologies validated in this study with the NMR data is the presence of adenosine (the purine nucleobase) at the 3′ end of the RNA dinucleoside monophosphates. The ApA and CpA dinucleosides thus possess a higher stacking ratio than the ApC or CpC ones. The calculated base-stacking ratio in the CpC molecule decreases as the temperature increase.

Acknowledgment. This work was supported by the Academy of Sciences of the Czech Republic, Grant Nos. IAA400550701, AV0Z50040507, AV0Z50520701, AV0Z40550506, and AV0Z50040702, and by the Grant Agency of Charles University, Grant GAUK No. 58708. V.S. was supported by a Human Frontier Science Program (HFSP) Young Investigator's Grant.

Supporting Information Available: Calculated trajectories and distribution functions for the α, β, γ, δ, ε, ζ, and χ torsion angles, trajectories of the geometry parameters for analysis of base stacking, and an explicit form of the Karplus equations. This material is available free of charge via the Internet at http://pubs.acs.org.

References and Notes

(1) Kruger, K.; Grabowski, P. J.; Zaug, A. J.; Sands, J.; Gottschling, D. E.; Cech, T. R. *Cell* **1982**, *31*, 147.
(2) Gesteland, R. F.; Cech, T. R.; Atkins, J. F. *Cold Spring Harbor Monograph Series*, 2006.
(3) Fire, A.; Xu, S. Q.; Montgomery, M. K.; Kostas, S. A.; Driver, S. E.; Mello, C. C. *Nature* **1998**, *391*, 806.
(4) Ban, N.; Nissen, P.; Hansen, J.; Moore, P. B.; Steitz, T. A. *Science* **2000**, *289*, 905.
(5) Wimberly, B. T.; Brodersen, D. E., Jr.; Morgan-Warren, R.; Carter, A. P.; Vonrhein, C.; Hartsch, T.; Ramakrishnan, V. *Nature* **2000**, *407*, 327.
(6) Schuwirth, B. S.; Borovinskaya, M. A.; Hau, C. W.; Zhang, W.; Vila-Sanjurjo, A.; Holton, J. M.; Cate, J. H. D. *Science* **2005**, *310*, 827.
(7) Selmer, M.; Dunham, C. M.; Murphy, F. V.; Weixlbaumer, A.; Petry, S.; Kelley, A. C.; Weir, J. R.; Ramakrishnan, V. *Science* **2006**, *313*, 1935.
(8) Harms, J.; Schluenzen, F.; Zarivach, R.; Bashan, A.; Gat, S.; Agmon, I.; Bartels, H.; Franceschi, F.; Yonath, A. *Cell* **2001**, *107*, 679.
(9) Korostelev, A.; Trakhanov, S.; Laurberg, M.; Noller, H. F. *Cell* **2006**, *126*, 1065.
(10) Tanaka, Y.; Taira, K. *Chem. Commun.* **2005**, 2069.
(11) Tanaka, Y.; Kasai, Y.; Mochizuki, S.; Wakisaka, A.; Morita, E. H.; Kojima, C.; Toyozawa, A.; Kondo, Y.; Taki, M.; Takagi, Y.; Inoue, A.; Yamasaki, K.; Taira, K. *J. Am. Chem. Soc.* **2004**, *126*, 744.
(12) Frank, J.; Agrawal, R. K. *Nature* **2000**, *406*, 318.
(13) Frank, J.; Spahn, C. M. T. *Rep. Prog. Phys.* **2006**, *69*, 1383.
(14) Mitra, K.; Frank, J. *Annu. Rev. Biophys. Biomol. Struct.* **2006**, *35*, 299.
(15) Li, P. T. X.; Vieregg, J.; Tinoco, I. *Annu. Rev. Biochem.* **2008**, *77*, 77.
(16) Spirin, A. S. *FEBS Lett.* **2002**, *514*, 2.
(17) Mathews, D. H.; Sabina, J.; Zuker, M.; Turner, D. H. *J. Mol. Biol.* **1999**, *288*, 911.
(18) Mathews, D. H.; Turner, D. H. *Curr. Opin. Struct. Biol.* **2006**, *16*, 270.
(19) Leontis, N.; Stombaugh, J.; Westhof, E. *Biochimie* **2002**, *84*, 961.
(20) Lescoute, A.; Leontis, N. B.; Massire, C.; Westhof, E. *Nucleic Acids Res.* **2005**, *33*, 2395.
(21) Sarver, M.; Zirbel, C. L.; Stombaugh, J.; Mokdad, A.; Leontis, N. B. *J. Math. Biol.* **2008**, *56*, 215.
(22) Klein, D. J.; Schmeing, T. M.; Moore, P. B.; Steitz, T. A. *EMBO J.* **2001**, *20*, 14.
(23) Nissen, P.; Ippolito, J. A.; Ban, N.; Moore, P. B.; Steitz, T. A. *Proc. Natl. Acad. Sci. U.S.A.* **2001**, *98*, 4899.
(24) Lescoute, A.; Westhof, E. *RNA* **2006**, *12*, 83.
(25) Kolk, M. H.; van der Graaf, M.; Wijmenga, S. S.; Pleij, C. W. A.; Heus, H. A.; Hilbers, C. W. *Science* **1998**, *280*, 434.
(26) Ferner, J.; Villa, A.; Duchardt, E.; Widjajakusuma, E.; Wohnert, J.; Stock, G.; Schwalbe, H. *Nucleic Acids Res.* **2008**, *36*, 1928.
(27) Schwalbe, H.; Buck, J.; Furtig, B.; Noeske, J.; Wohnert, J. *Angew. Chem., Int. Ed.* **2007**, *46*, 1212.
(28) Varani, G.; Aboulela, F.; Allain, F. H. T. *Prog. Nucl. Magn. Reson. Spectrosc.* **1996**, *29*, 51.
(29) Getz, M.; Sun, X. Y.; Casiano-Negroni, A.; Zhang, Q.; Al-Hashimi, H. M. *Biopolymers* **2007**, *86*, 384.
(30) Flinders, J.; Dieckmann, T. *Prog. Nucl. Magn. Reson. Spectrosc.* **2006**, *48*, 137.
(31) Tanaka, Y.; Ono, A. *Dalton Trans.* **2008**, 4965.
(32) Li, W.; Frank, J. *Proc. Natl. Acad. Sci. U.S.A.* **2007**, *104*, 16540.
(33) Rhodes, M. M.; Reblova, K.; Sponer, J.; Walter, N. G. *Proc. Natl. Acad. Sci. U.S.A.* **2006**, *103*, 13380.
(34) Rázga, F.; Koča, J.; Mokdad, A.; Šponer, J. *Nucleic Acids Res.* **2007**, *35*, 4007.
(35) McDowell, S. E.; Spackova, N.; Sponer, J.; Walter, N. G. *Biopolymers* **2007**, *85*, 169.
(36) Auffinger, P.; Hashem, Y. *Curr. Opin. Struct. Biol.* **2007**, *17*, 325.
(37) Qin, P. Z.; Dieckmann, T. *Curr. Opin. Struct. Biol.* **2004**, *14*, 350.
(38) Bock, L. C.; Griffin, L. C.; Latham, J. A.; Vermaas, E. H.; Toole, J. J. *Nature* **1992**, *355*, 564.
(39) Furtig, B.; Richter, C.; Wohnert, J.; Schwalbe, H. *ChemBioChem* **2003**, *4*, 936.
(40) Přecechtělová, J.; Padrta, P.; Munzarová, M. L.; Sklenář, V. *J. Phys. Chem. B* **2008**, *112*, 3470.
(41) Wijmenga, S. S.; van Buuren, B. N. M. *Prog. Nucl. Magn. Reson. Spectrosc.* **1998**, *32*, 287.
(42) Grzesiek, S.; Barfield, M.; Cordier, F.; Dingley, A.; Feigon, J.; Nicholson, L. K. *Abstr. Pap. Am. Chem. Soc.* **2000**, *219*, U139.
(43) Grzesiek, S.; Cordier, F.; Jaravine, V.; Barfield, M. *Prog. Nucl. Magn. Reson. Spectrosc.* **2004**, *45*, 275.
(44) Karplus, M. *J. Chem. Phys.* **1959**, *30*, 11.
(45) Karplus, M. *J. Am. Chem. Soc.* **1963**, *85*, 2870.

(46) Sychrovský, V.; Vokáčová, Z.; Šponer, J.; Špačková, N.; Schneider, B. *J. Phys. Chem. B* **2006**, *110*, 22894.

(47) Rinnenthal, J.; Richter, C.; Ferner, J.; Duchardt, E.; Schwalbe, H. *J. Biomol. NMR* **2007**, *39*, 17.

(48) Ravindranathan, S.; Kim, C. H.; Bodenhausen, G. *J. Biomol. NMR* **2003**, *27*, 365.

(49) Norberg, J.; Nilsson, L. *J. Am. Chem. Soc.* **1995**, *117*, 10832.

(50) Case, D. A.; Darden, T. A.; Cheatham, T. E., III; Simmerling, C. L.; Wang, J.; Duke, R. E.; Luo, R.; Merz, K. M.; Wang, B.; Pearlman, D. A.; Crowley, M.; Brozell, S.; Tsui, V.; Gohlke, H.; Mongan, J.; Hornak, V.; Cui, G.; Beroza, P.; Schafmeister, C.; Caldwell, J. W.; Ross, W. S.; Kollman, P. A. *AMBER 8*; University of California: San Francisco, CA, 2004.

(51) Wang, J. M.; Cieplak, P.; Kollman, P. A. *J. Comput. Chem.* **2000**, *21*, 1049.

(52) Marino, J. P.; Schwalbe, H.; Griesinger, C. *Acc. Chem. Res.* **1999**, *32*, 614.

(53) Yokoyama, S.; Inagaki, F.; Miyazawa, T. *Biochemistry* **1981**, *20*, 2981.

(54) Haasnoot, C. A. G.; Deleeuw, F.; Altona, C. *Tetrahedron* **1980**, *36*, 2783.

(55) Munzarová, M. L.; Sklenář, V. *J. Am. Chem. Soc.* **2003**, *125*, 3649.

(56) Berman, H. M.; Olson, W. K.; Beveridge, D. L.; Westbrook, J.; Gelbin, A.; Demeny, T.; Hsieh, S.-H.; Srinivasan, A. R.; Schneider, B. *Biophys. J.* **1992**, *63*, 751.

(57) Richardson, J. S.; Schneider, B.; Murray, L. W.; Kapral, G. J.; Immormino, R. M.; Headd, J. J.; Richardson, D. C.; Ham, D.; Hershkovits, E.; Williams, L. D.; Keating, K. S.; Pyle, A. M.; Micallef, D.; Westbrook, J.; Berman, H. M. *RNA* **2008**, *14*, 465.

(58) Schneider, B.; Morávek, Z.; Berman, H. M. *Nucleic Acids Res.* **2004**, *32*, 1666.

(59) Svozil, D.; Kalina, J.; Omelka, M.; Schneider, B. *Nucleic Acids Res.* **2008**, *36*, 3690.

(60) Krasovská, M. V.; Šefčíková, J.; Réblová, K.; Schneider, B.; Walter, N. G.; Šponer, J. *Biophys. J.* **2006**, *91*, 626.

(61) Réblová, K.; Lankaš, F.; Rázga, F.; Krasovská, M. V.; Koča, J.; Šponer, J. *Biopolymers* **2006**, *82*, 504.

(62) Gabb, H. A.; Sanghani, S. R.; Robert, C. H.; Prévost, C. *J. Mol. Graphics* **1996**, *14*, 6.

(63) Sychrovský, V.; Muller, N.; Schneider, B.; Smrecki, V.; Špirko, V.; Šponer, J.; Trantírek, L. *J. Am. Chem. Soc.* **2005**, *127*, 14663.

(64) Munzarová, M. L.; Sklenář, V. *J. Am. Chem. Soc.* **2002**, *124*, 10666.

(65) Norberg, J.; Nilsson, L. *J. Phys. Chem.* **1995**, *99*, 13056.

JP809762B